SANDIA REPORT
SAND2012-8023
Unlimited Release
Printed Month and Year

Magneto-hydrodynamic detection of vortex shedding for molten salt flow sensing

Alan M. Kruizenga, Robert Crocker

Prepared by
Sandia National Laboratories
Albuquerque, New Mexico 87185 and Livermore, California 94550

Sandia National Laboratories is a multi-program laboratory managed and operated by Sandia Corporation, a wholly owned subsidiary of Lockheed Martin Corporation, for the U.S. Department of Energy's National Nuclear Security Administration under contract DE-AC04-94AL85000.

Issued by Sandia National Laboratories, operated for the United States Department of Energy by Sandia Corporation.

Available to DOE and DOE contractors from
U.S. Department of Energy
Office of Scientific and Technical Information
P.O. Box 62
Oak Ridge, TN 37831

Telephone: (865) 576-8401
Facsimile: (865) 576-5728
E-Mail: reports@adonis.osti.gov
Online ordering: http://www.osti.gov/bridge

Available to the public from
U.S. Department of Commerce
National Technical Information Service
5285 Port Royal Rd.
Springfield, VA 22161

Telephone: (800) 553-6847
Facsimile: (703) 605-6900
E-Mail: orders@ntis.fedworld.gov
Online order: http://www.ntis.gov/help/ordermethods.asp?loc=7-4-0#online

SAND2012-8023
Unlimited Release
Printed Month Year

Magneto-hydrodynamic detection of vortex shedding for molten salt flow sensing

Alan M. Kruizenga*, Robert Crocker**
*Materials Chemistry 8223, **
Advanced Systems Engineering and Deployment 8125
Sandia National Laboratories
P.O. Box 0969
Livermore, California 94550-MS9403

Abstract

High temperature flow sensors must be developed for use with molten salts systems at temperatures in excess of 600°C. A novel magneto-hydrodynamic sensing approach was investigated. A prototype sensor was developed and tested in an aqueous sodium chloride solution as a surrogate for molten salt. Despite that the electrical conductivity was a factor of three less than molten salts, it was found that the electrical conductivity of an electrolyte was too low to adequately resolve the signal amidst surrounding noise. This sensor concept is expected to work well with any liquid metal application, as the generated magnetic field scales proportionately with electrical conductivity.

ACKNOWLEDGMENTS

This author would like to thank the LDRD office for the funding to make this work possible. I also want to acknowledge the excellent conversations of Nathan Siegal, Robert Bradshaw and David Gill over the course of this work. Their insight and suggestions have proved to be very encouraging and thought provoking.

CONTENTS

FIGURES

TABLES

NOMENCLATURE

CSP	Concentrated Solar Power
DOE	Department of Energy
Cl	Chloride
Na	Sodium
St	Strouhal number
V	Velocity
f	frequency
L	length scale
J	Current density
E	Electric field
B_o	Initial magnetic field
B_i	Secondary magnetic field
MHD	Magneto Hydro Dynamic
EES	Engineering Equation Solver
ρ	Density
σ	Electric conductivity

1. INTRODUCTION

Developers of concentrated solar power (CSP) are aggressively pursuing SunShot, an initiative begun in 2011 by the U.S. Department of Energy [1]. The goal is for CSP to become cost-competitive with fossil energy, without any form of subsidy. This will require nearly all aspects related to plant costs, both capital and operating, to decrease by more than a factor of three [2].

Among the major areas targeted for research are thermal energy storage and thermodynamic efficiency. Inherently, as the upper temperature limit increases so does the overall cycle efficiency, in accordance with Carnot's law. Cycles with a maximum temperature range of 800-900°C are projected to have cycles that operate with 50% efficiency or more [3]. Unfortunately, this dictates that previously developed technology for monitoring system conditions is not adequate for such high temperatures.

Seemingly trivial measurements, such as flow rate and pressure drop, were identified as no longer being commercially viable for high temperature molten salt systems. Molten salts are integral to many industries with common examples being aluminum refining (alumina in molten cryolyte) and glass production (silicates, carbonates, sulfates) [4]. Aluminum processing occurs between 900-1000°C where electrolysis, coupled with buoyant forces, is employed to separate the metal from the salt melt; hence no flow measurement of the hot fluid is required. In a flowing system, such as a central solar receiver, the measurement of the hot fluid flow is important from the standpoint of system control and monitoring.

The purpose of this document is to report on experiments and designs toward designing a high temperature flow sensor. The concept, relevant experiments, and results are reported within this paper.

2. CONCEPT

Many fluid flow sensing applications are based on the detection of periodic vortex shedding phenomena, also known as von Karman vortex streets [5]. An example of this phenomenon in nature is the periodic back and forth motion of an antenna or power line in high speed winds as vortices are shed from one side then the other. This phenomenon is characterized by a non-dimensional group, which relates the shedding frequency to velocity:

$$\mathbf{St} = \frac{\mathbf{fL}}{\mathbf{V}} \qquad \text{Equation 1}$$

In the definition of the Strouhal number, St, f is the frequency of oscillations, V is the velocity and L is the length of interest, which seemingly varies from author to author, but is typically defined as the width of the bluff body obstructing the flow. There are many factors that need to be considered in both the design and detection schemes for vortex shedding applications. Flow rate, bluff body design, and flow blockage area ratios are all found to influence the Strouhal number and associated response parameters [5-11].

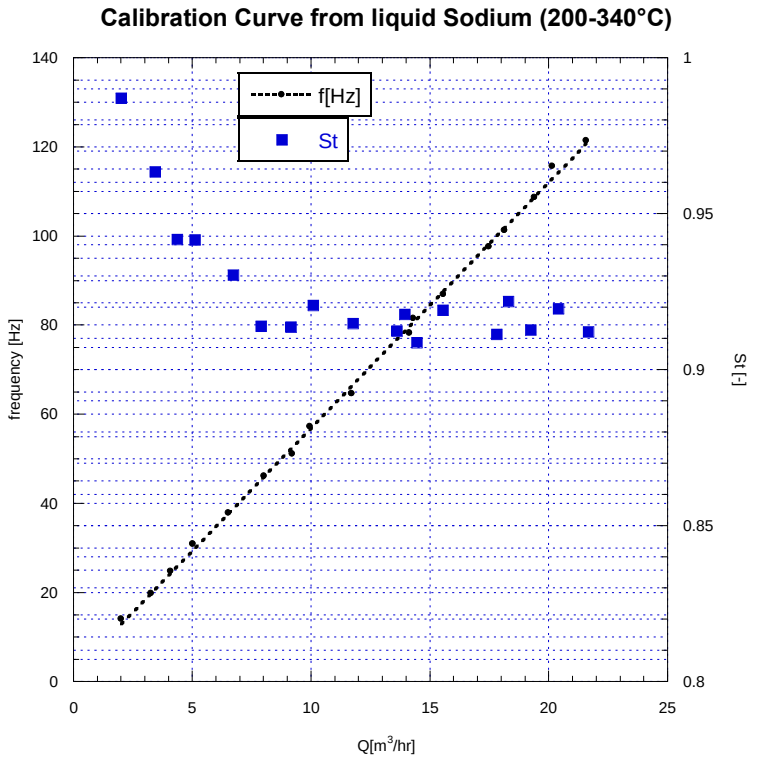

Figure 1: Flow rate vs. Strouhal number for liquid sodium (200-340 °C) Reproduced from [12].

Most industrially available methods employ detection of either pressure oscillations in the fluid, or force and stress induced on the bluff body or force plate [5, 6]. The frequency response is

detected and correlated to the velocity flow response of the sensor. The unfortunate situation is the failure of most detection schemes, mentioned here and elsewhere, at the elevated temperatures of molten salts for a variety of reasons. Novel electrostatic and electromagnetic schemes were proposed in literature, but few have been proven in an aggressive environment [9, 12-14]. A magneto-hydrodynamic technique with an inductive detector to sense flow rates in ionic fluids was explored, where the concept was successfully applied to liquid sodium [12] It was observed that the Strouhal number was non-linear at lower volumetric flow rates, due to strong interaction between the Lorentz forces and Karman vortices.

The electromagnetic induction principle is diagrammed in figure 2 and the detection arrangement is depicted in figure 3. An electrolyte is a fluid having freely mobile charged ions, e.g., sodium chloride in water where the salt is dissociated into Na^+ cations and Cl^- anions. In the absence of a solid-liquid interface, there is no net charge density in the fluid at classical physics scales. Flow of an electrolyte does not in itself constitute an electrical current, since equal quantities of positive and negative charge are flowing together.

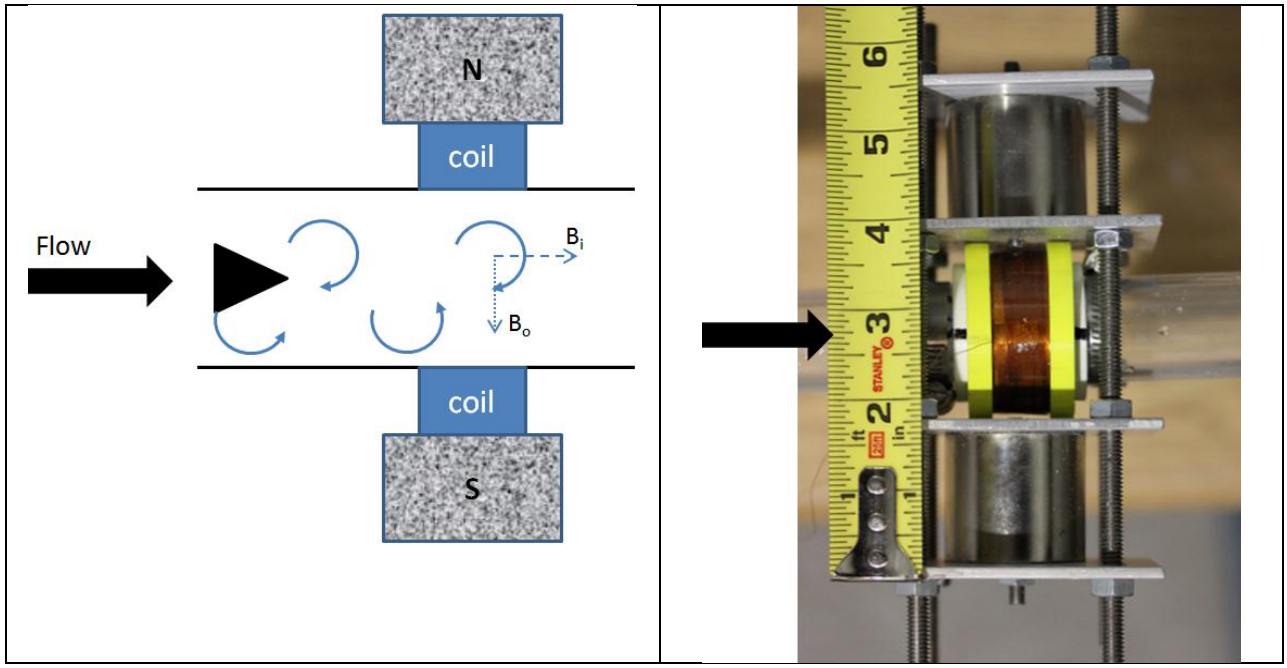

Figure 2: Sensor schematic and set up

In the present sensor arrangement, shown in figure 2, an electrolyte flows in the x-direction past a bluff body which creates a von Karman street of periodically alternating rotating fluid vortices. The magnetic induction field, created by neodymium magnets, is oriented perpendicular to the flow and vortex rotation axis. A sensing coil is placed parallel to the flow in the induction zone.

Consider the single vortex diagrammed in figure 3. The velocity vectors of the vortices are in the xy-plane. The vortices translate with the flow through a magnetic field oriented in the y--direction. The magnetic field gives rise to Lorentz forces directed in the z-direction, $\vec{F} = q(\vec{v} \times \vec{B})$, that polarize the mobile ionic charges flowing with the electrolyte. The velocity components parallel to the magnetic field in the y-direction are not influenced. However, the opposing fluid

velocities, ± v_x, on either side of the vortex result in opposite charge polarizations, with corresponding electrical fields. The proximal, opposing electrical fields create *electrical* eddy currents in the yz plane consistent with the generalized Ohm's law:

$$\vec{\mathbf{J}} = -\boldsymbol{\sigma} \cdot \vec{\mathbf{E}}, \textbf{and continuity}, \nabla \cdot \vec{\mathbf{J}} = \mathbf{0} \qquad \text{Equation 2}$$

In accordance with the Maxwell – Faraday law, $\nabla \times \vec{E} + \frac{\partial \vec{B}}{\partial t} = 0$, there is an induced transient magnetic field parallel to the curl axis of the electrical eddies. This induced magnetic field is oriented in the x-direction, parallel to the electrolyte flow. A solenoid winding around the flow axis is used to detect the transient magnetic field as shown in figure 2. The periodicity of the magnetic field corresponds to the vortex shedding period as the vortex rotation direction alternates. Essentially, the detector is sensitive to the perturbations parallel to the main flow caused by the vortices. The magnitude of the induced magnetic field is directly related to the rotation speed of the vortex magnitude and the conductivity of the fluid.

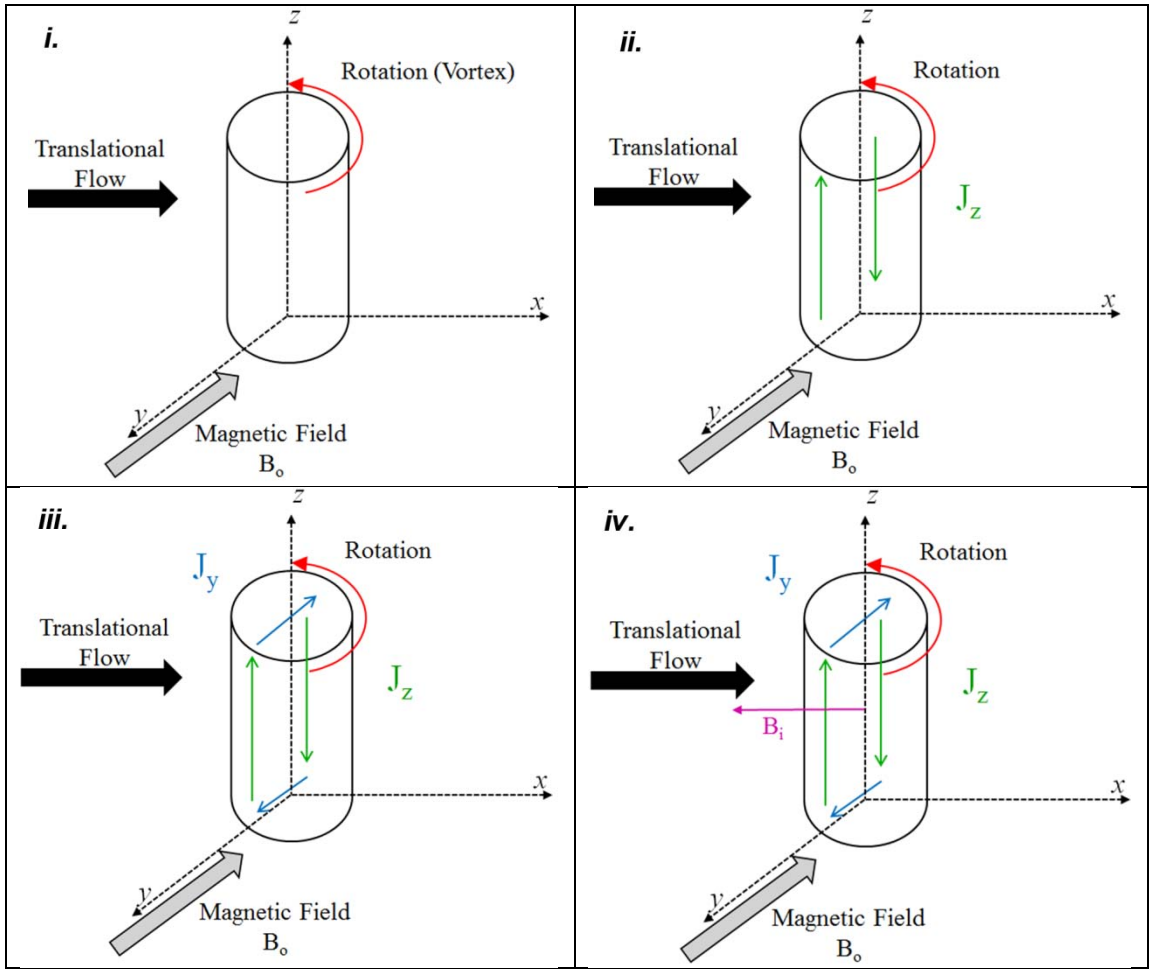

Figure 3: i. Initial vortex induced by bluff body. ii. Interaction of rotating, conducting fluid causes a Lorentz induced current in z direction (J_z). iii. Due to $\cdot \nabla \cdot \mathbf{J} = 0$, there can be no current source in the vortex, hence J_y is induced (closes the current loop). iv. The current acts similarly to a wire and induces a secondary magnetic field parallel to the translational direction.

The inherent advantage of this type of a sensor can be realized at high temperatures, as the transducer is external to the pipe and can be thermally isolated from the flow. Parameters to consider for the fluid of interest should include the Reynolds number (standard, *Re*, and magnetic, Re_m), magnetohydrodynamic (MHD) interaction parameter, *N*, as presented in table 1.

Table 1: Relevant Dimensionless Numbers

Parameter	Sodium [400°C]	Lead [400°C]	Water [25°C, 101kPa]	NaCl solution [25°C, 20 wt%]	Equimolar Solar Salt [500°C]
Viscosity ν [Pa-sec]	0.28E-3[1]	2.3E-3[1]	0.89E-3[1]	1.38E-3[1]	1.3E-3[4]
Density ρ [kg/m^3]	971[2] (25°C)	10,600[2]	997[1]	1,144[1]	1,774[4]
Conductivity σ [S/m]	4.5E+6[2]	9.9E+5[2]	5.5E-6[2]	20.4[3]	59[5]
Reynolds No. Re[-]	348E+3	466E+3	111E+3	83E+3	136E+3
MHD parameter N[-]*	18.64	0.37	2.2e-11	7.1e-5	13.2E-5
Reynolds No. (mag) Re_m[-]*	0.57	0.12	7E-13	3E-6	7E-6
$Re_m = \mu_o \sigma V_o D_o$, $N = \sigma B_o^2 D_o / \rho V_o$;					
μ_o – magnetic permeability in a vacuum, V_o=1[m/s], D_o=0.1[m] , B_o=0.2[T]					
1 - ref [15], 2 - ref [16], 3 - ref [17], 4 - ref [18], 5 - ref [19]					

3. EXPERIMENTAL APPROACH

This sensor concept has been proven through use with liquid sodium, thus it is of interest to determine whether the induced secondary field could be detected in molten salts, such as nitrate salts used in the thermal solar power industry. Aqueous NaCl was chosen as a convenient surrogate fluid to allow for tests to be performed at room temperature since the MHD interaction parameter is of the same magnitude as the equimolar solar salt, additionally the electrical conductivity was within a factor of three. The flow loop consisted of a high flow rate pump (SHURFlo, Noryl 24669), capable of 33*GPM* at 10*ft/s* flow rate and maximum head of 68*ft*. Flow was controlled by various throttle valves as shown in Figure 4. Flow through the test section was monitored using a turbine flow meter with an accuracy of ±1% of the reading (Omega, FTB-1425).

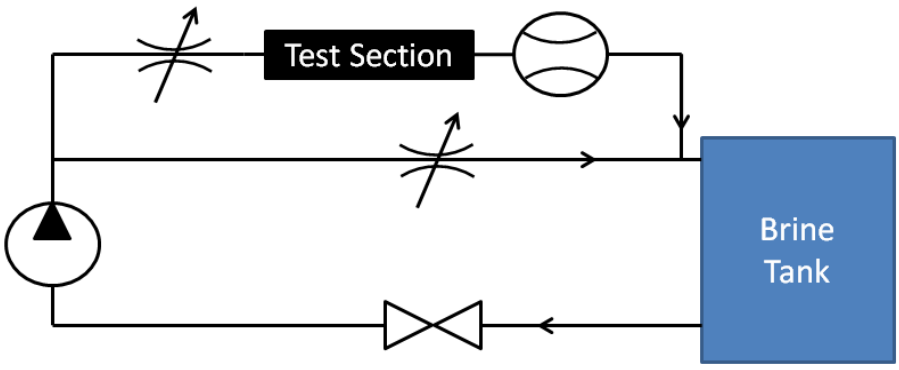

Figure 4: Schematic of Flow loop

3.1. Sensor Design / Detection Electronics

The sensor is comprised of two permanent neodymium rare earth magnets (K J Magnetics, Inc., model RX84X8), which have a maximum residual flux density of 13,200 *gauss* (1.32 *T*). While this value is appears quite high, in practice the field is much lower as it will decrease with inverse square of distance from the magnet. While the molten salt temperature is well above the Curie temperature of the magnets, high-permeability pole pieces can be used to direct the magnetic field circuit through the sensor.

The inductive pick-up sensor is an air-core solenoid comprised of 34AWG magnet wire, which forms a 140*mH* inductor used for detection of the secondary magnetic field. This inductor was mounted in conjunction with the permanent magnets (Figure 2), which was attached to the outside of the fluid flow pipe.

The detection electronics employed a current amplifier (SRS, Model SR570), which was connected to a data acquisition device (National Instruments, CompactDAQ cDAQ-9174, Module 9205). Labview software for frequency analysis of the time averaged signal via a fast Fourier transform was used, several windowing functions were investigated, but ultimately the

Hanning window was used during the measurements. Although the current amplifier had a built in band pass, high, and low pass signal filter, no signal modification was used in an effort to avoid accidental filtering out of the signal of interest.

3.2. Results and Discussion

As an initial confirmation of the measurement technique, a "solid vortex" was used. The solid vortex was cylindrical aluminum stock with a hole drilled through it and mounted on a shaft within the sensor cavity. This cylinder was then spun using a belt driven by a Dremel tool to simulate vortex rotation, with a photo of the setup in Figure 5. The observed signal was vastly larger than the surrounding noise (Figure 6). Unique frequencies were observed for two rotational speeds at about 150Hz and 225Hz. Higher order harmonics can also be observed in the detection software. During vibrational transients, in addition to audible chattering, a large amount of noise was observed at low frequencies. This could simulate incoherent vortex behavior, as the vibrations of lower frequencies were evident during excursions.

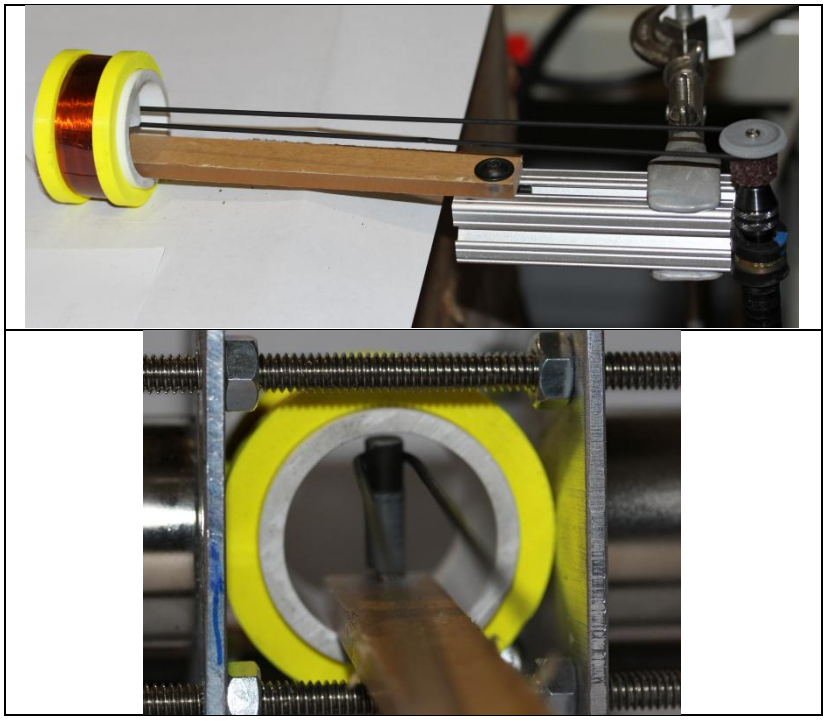

Figure 5: Simulated Solid vortex experiment

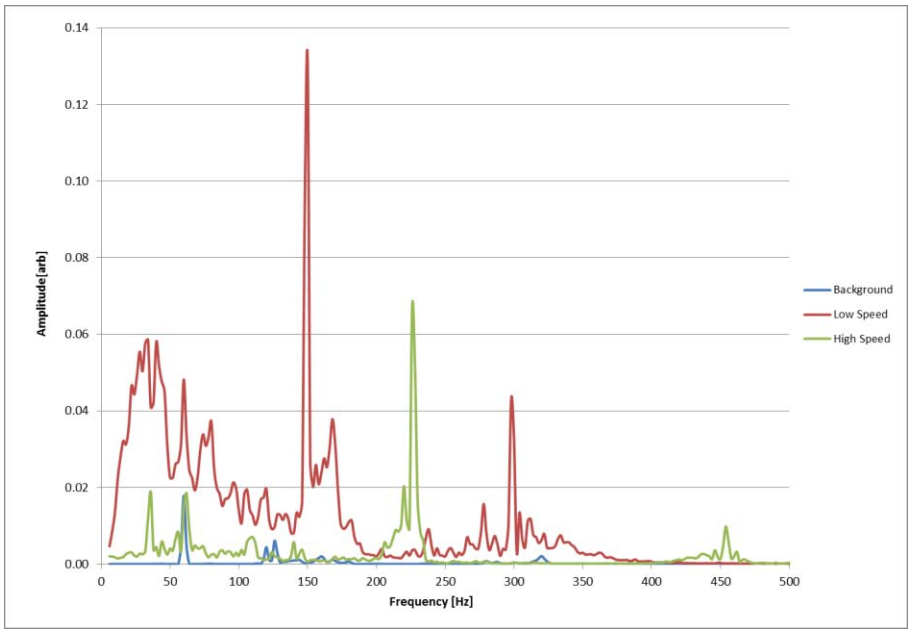

Figure 6: Results of solid vortex experiment. Dominant frequencies were observed at 150Hz and 225Hz for two speeds. Harmonics were observed, along with noise from audible chattering of the aluminum stock.

3.2.2. Bluff body and stroboscope detection

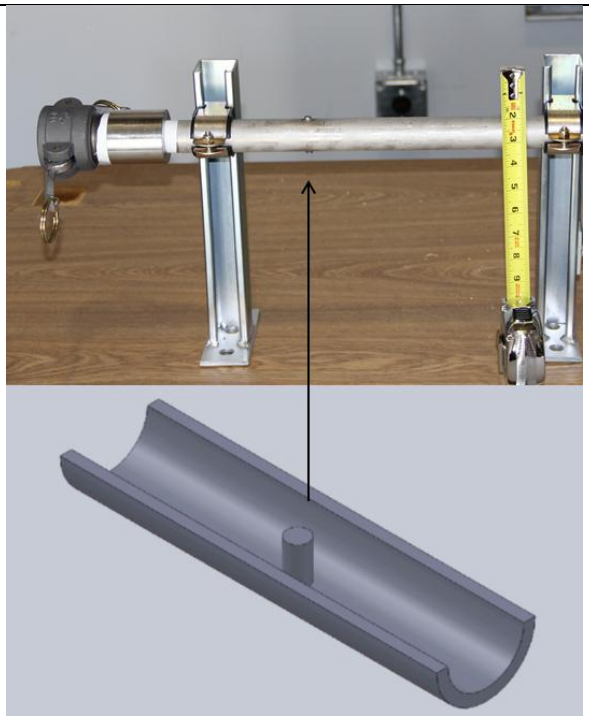

Figure 7: First prototype, utilizing a cylinder bluff body. Top is setup and bottom is a cutaway drawing.

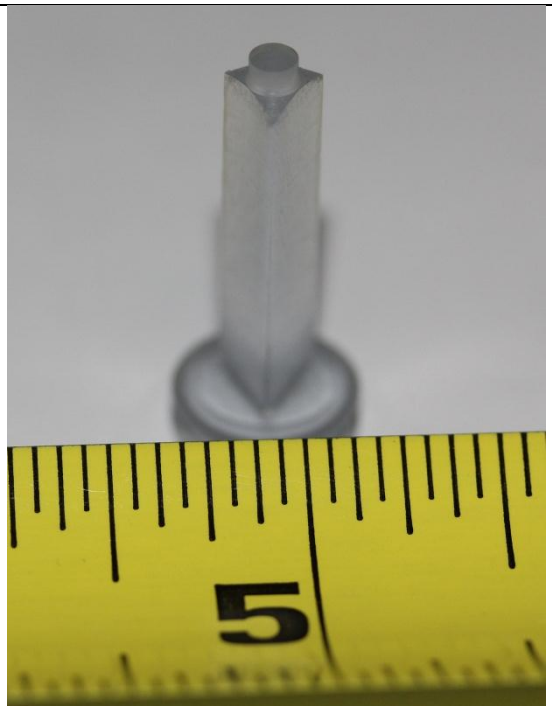

Figure 8: Prototype 2; equilateral triangle body.

Two prototype designs were tested during the experiments. The first prototype was fabricated from one inch schedule 40 stainless steel pipe (Figure 7) and a 0.25 inch cylinder bluff body, which was welded into place. It was found that noise from the surrounding environment was a problem. The problem was exacerbated by the expectation that all the noise observed (40-300Hz) was within the range of the shedding frequency. This problem was mitigated by making background noise measurements, which were found to be consistent in time (Figure 9). Background measurements were used to subtract or normalize measurements taken in the flow channel. Despite the efforts to remove background noise no apparent response signal was observed versus a variety of flow rates.

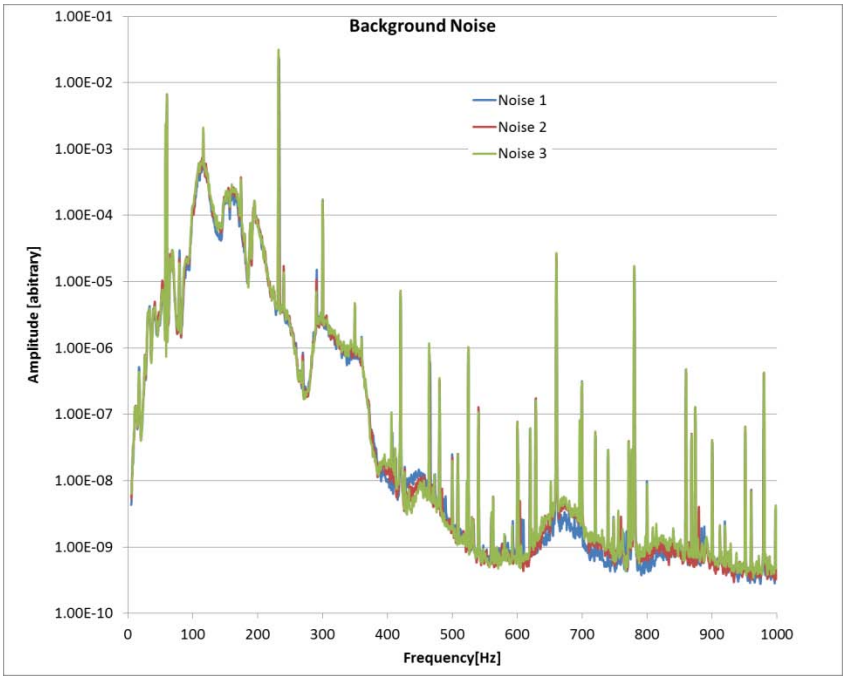

Figure 9: Background noise measurements

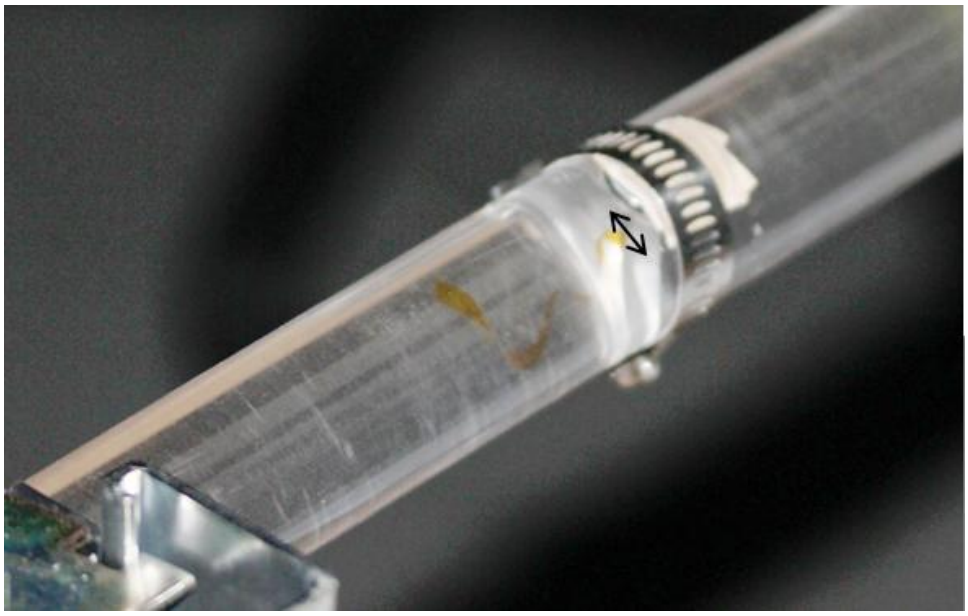

Figure 10: Orange color is a polyimide thin film affixed to wake region of a triangular bluff body. A stroboscope was used to determine shedding frequency.

A second experimental prototype was fabricated from clear acrylic tube, with an equilateral triangle bluff body (0.25 inch per face) made from PVC. (Figure 8) The bluff body was held in place with a pipe clamp to allow flexibility in changing bluff designs and orientation relative to the flow. This allowed the opportunity to affix a thin film to the wake region of the bluff body and measure the shedding frequency (Figure 10). The shedding frequency was measured using a stroboscope (Nova-Strobe bax Monarch) and was found to have a linear response when compared to a turbine flow meter (Figure 11).

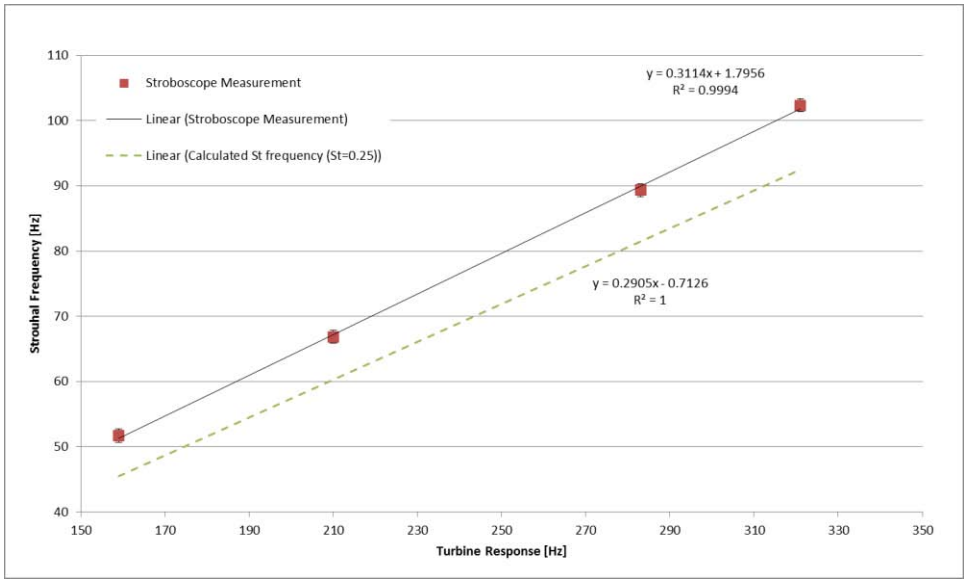

Figure 11: Measured shedding frequency compared to an assumed Strouhal number of 0.25.

Despite knowledge of the shedding frequency, allowing a detailed examination of frequencies in question, there was no apparent response from the inductive sensor. There are several likely reasons for this result. The first, and most probable, explanation for this phenomenon is that the electrical conductivity of the NaCl solution is too low, such that the MHD interaction parameter (*N*) and magnetic Reynolds number are too low to warrant a sufficient MHD response. Previous experiments that confirmed the method were performed in liquid sodium, where the MHD number varied from 0.5 - 4, due to variation in the volumetric flow (2-20m^3/hr) and magnetic field (0.04-0.09*T*) [12]. Correspondingly, the magnetic Reynolds number varied from 1.75 to 0.05. While both of these parameters will surely give some insight into the overall amplitude response of the secondary magnetic field, a more useful thought experiment may be employed for clarity.

Table 2: Ratio of conductivity over density for selected fluids

Fluid	σ/ρ[S-m^2/kg]	σ[S/m]	ρ[kg/m^3]
Sodium	4660	4.5e6[2]	970[2*]
Gallium	970	5.7e6[2]	5900[2]
Wood Metal	240	2.3e6[2]	9580[2]
Lead	93	0.9e6[2]	10600[2]
Mercury	58	0.7e6[2]	12750[1]
Equimolar Na,K//NO_3	0.033	59[3]	1770[3]
NaCl brine (20% by mass)	0.018	20[4]	1140[1]
Water	5e-9	5e-6[2]	997[1]
1 - ref[15], 2 - ref[16], 3 - ref[18], 4 - ref[17] **Density near room temperature*			

Consider Figure 3, step *ii*. The secondary magnetic field is primarily driven by a large J_z, which is a combination of electrical conductivity of the fluid and the velocity in the z direction. Hence, J_z will be maximized by maximizing the electrical conductivity and V_z. Minimizing the fluid density will also minimize moment of inertia such that J_z would increase by an increase in the vortex rotational velocity, V_z. Sodium is the ideal liquid owing to the relatively low density, especially in view of other metals, and high electrical conductivity.

Table 2 has a list of some potential fluids and their relevant properties. Sodium has far and away the best ratio of σ/ρ, which makes it intuitive why the sensor worked so well with that fluid. Gallium is close behind with a ratio of about five times less than sodium. Other metals listed were at least one or more orders of magnitude below sodium. The ratio σ/ρ for molten salts and brine solutions is ~100,000 times smaller than the ratio for sodium, which illustrates one likely reason for the inability of the detector to pick up the induced fields.

Use of a Hall type sensor was ruled out [20] as a simple Lorentz calculation determined the relative field strength was 6 to 7 orders of magnitude smaller than the excitation field (Figure 12). It is clear from this calculation why liquid sodium worked well in previous studies. Applications where liquid metal flow must be monitored, such as in advanced nuclear reactor concepts or in foundries, may utilize this sensing concept.

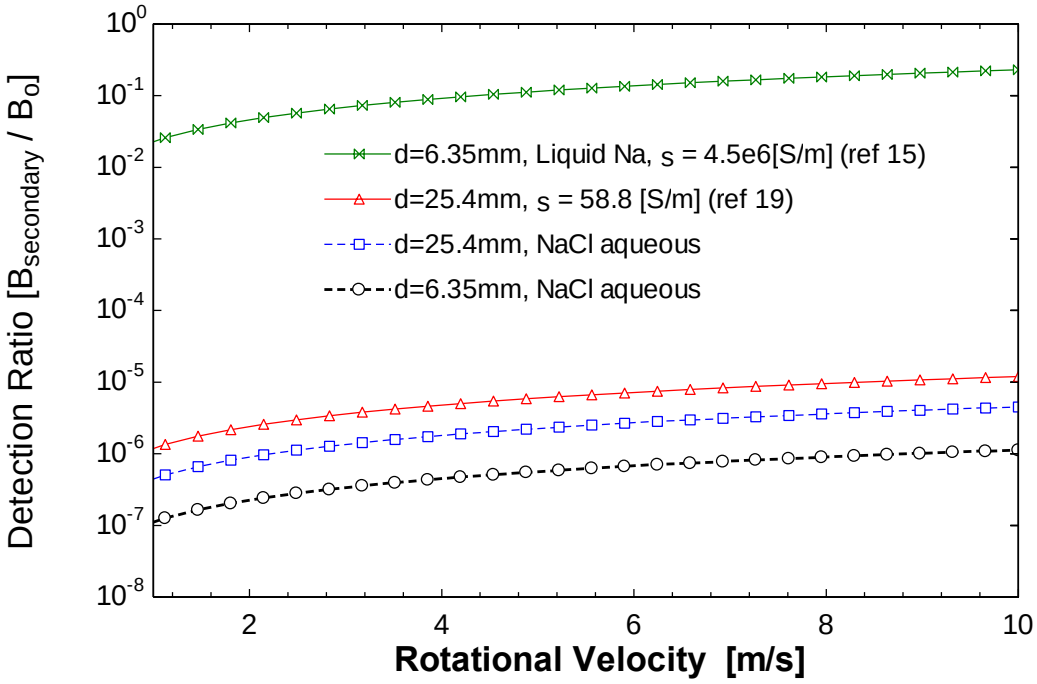

Figure 12: Lorentz calculation for rotational velocity and effect of electrical conductivity

4. CONCLUSIONS:

The calculations and experiments toward development of a high temperature flow sensor were presented. Experiments determining vortex shedding behavior were confirmed and indicate inadequate signal to noise response.

An MHD detector may work for a molten salt flow; however a large magnetic field would need to be induced across the flow channel. Such a large magnetic field may have harmful and unforeseen effects in an industrial setting. Practical limits to the field strength due to the degraded permeability with temperature would likely be reached.

This sensing approach would still be a possible solution for high temperature flows as the sensor components would be located externally to the flow. The application could be realized by active cooling or appropriate insulation to lower the sensor temperature.

Future studies should seek to study different ratios of σ/ρ, where the best secondary response should be expected from a maximization of this value. It would be interesting to understand which non-dimensional parameter primarily governs the response of the sensor, and furthermore, it would be of interest to understand the practical, detectable limit.

5. REFERENCES

1. *SunShot Initiative*. 2011 [cited 2011; Available from: http://www1.eere.energy.gov/solar/sunshot/.
2. Gary, J., C. Turchi, and N.P. Siegel, *CSP and the SunShot Initiative*, in *SolarPACES*2011, SolarPACES: Granada, Spain.
3. Stekli, J., *Thermal Energy Storage and the United States Department of Energy's SunShot Initiative*, in *SolarPACES*2011, SolarPACES: Granada, Spain.
4. Lovering, D.G., *Molten salt technology*1982, New York: Plenum Press.
5. Baker, R.C., *Flow measurement handbook: industrial designs, operating principles, performance, and applications*2000, New York: Cambridge University Press. 524.
6. Venugopal, A., A. Agrawal, and S.V. Prabhu, *Review on vortex flowmeter - Designer perspective.* Sensors and Actuators, A: Physical, 2011. **170**(1-2): p. 8-23.
7. El Wahed, A.K., M.W. Johnson, and J.L. Sproston, *Numerical study of vortex shedding from different shaped bluff bodies.* Flow Measurement and Instrumentation, 1993. **4**(4): p. 233-240.
8. Venugopal, A., A. Agrawal, and S.V. Prabhu, *Influence of blockage and shape of a bluff body on the performance of vortex flowmeter with wall pressure measurement.* Measurement: Journal of the International Measurement Confederation, 2011. **44**(5): p. 954-964.
9. Bera, S.C., J.K. Ray, and S. Chattopadhyay, *A modified inductive pick-up type technique of measurement in a vortex flowmeter.* Measurement: Journal of the International Measurement Confederation, 2004. **35**(1): p. 19-24.
10. Reik, M., et al., *Flow rate measurement in a pipe flow by Vortex shedding.* Forschung im Ingenieurwesen/Engineering Research, 2010. **74**(2): p. 77-86.
11. Yamasaki, H., *Progress in hydrodynamic oscillator type flowmeters.* Flow Measurement and Instrumentation, 1993. **4**(4): p. 241-247.
12. Adamovskii, L.A., *Vortex electromagnetic flow meters for liquid metal coolants.* Measurement Techniques, 2007. **50**(1): p. 58-65.
13. El Wahed, A.K. and J.L. Sproston, *The influence of shedder shape on the performance of the electrostatic vortex flowmeter.* Flow Measurement and Instrumentation, 1991. **2**: p. 11.
14. Sproston, J.L., A.K. El Wahed, and M.W. Johnson, *An electrostatic vortex shedding meter.* Flow Measurement and Instrumentation, 1990. **1**: p. 8.
15. F-Chart Software, w.f.c., *EES - Engineering Equation Solver*, 2010.
16. *Material Property Data*. 2012 [cited 2012; Available from: http://www.matweb.com/.
17. *CRC Handbook of Chemistry and Physics*, W.M. Haynes, Editor 2012.
18. Nissen, D.A., *Thermophysical properties of the equimolar mixture sodium nitrate-potassium nitrate from 300 to 600.degree.C.* Journal of Chemical & Engineering Data, 1982. **27**(3): p. 269-273.
19. Coastal Chemical Co., L.L.C., *Hitec Solar Salt*.
20. Chiesi, L., et al., *Chopping of a weak magnetic field by a saturable magnetic shield.* Sensors and Actuators, A: Physical, 1997. **60**(1-3): p. 5-9.

APPENDIX A: CALCULATIONS

Simple Lorentz calculations were performed to determine the relative magnitude of magnetic fields needed. The calculations were done using equations in Figure 13 and in the program Engineering Equation Solver (EES).

These calculations were done to motivate the use of a unidirectional magnetic detection scheme (i.e. inductive methods versus a hall type method).

$\sigma = 4.5 \times 10^{6}$ Units S/m or $C^2/s\text{-}m^2\text{-}N$ electrical conductivity

$E = 0$ Electric field set to zero

$B = 0.1$ [N*s/C-m] Magnetic field in Tesla

velocity in parametric table

$J = \sigma \cdot (E + v \cdot B)$ Current Density

$I_z = J \cdot A$ Current

$A = L \cdot \frac{d}{2}$ Area to be half of the vortex

$L = 4 \cdot d$ Length 4 times longer than diameter

$d = 0.00635$ [m] diameter assumed to be the same as bluff body

$B_{secondary} = \mu_o \cdot \frac{I_z}{\pi \cdot d}$ Induced Magnetic field - assumption used long wire with steady current solution

$\mu_o = 4 \cdot \pi \cdot 10^{-7}$ permeability of free space

$B_r = \frac{B_{secondary}}{B}$ Induced magnetic field normalized by initial field strength

Figure 13: Equations and constants used in calculations

DISTRIBUTION

1	MS0124	Robert Hwang	8004	(electronic copy)
1	MS1127	David Gill	6123	(electronic copy)
1	MS1127	James Pacheco	6123	(electronic copy)
1	MS9292	Robert Crocker	8125	(electronic copy)
1	MS9153	Timothy Shepodd	8220	(electronic copy)
1	MS9403	Alan Kruizenga	8223	(electronic copy)
1	MS9403	Adam Rowen	8223	(electronic copy)
1	MS0899	Technical Library	9536	(electronic copy)
1	MS0359	D. Chavez, LDRD Office	1911	(electronic copy)


Sandia National Laboratories